Electronic Supplementary Material (ESI) for Energy & Environmental Science.

Structural and Optical Properties of MethylammoniumLead Triiodide Across the Tetragonal to Cubic Phase Transition: Implications for Perovskite Solar Cells

Claudio Quarti,[a,b,*] Edoardo Mosconi,[a] James M. Ball,[c] Valerio D'Innocenzo,[c,d] Chen Tao,[c] Sandeep Pathak,[e] Henry J. Snaith,[e] Annamaria Petrozza,[c] Filippo De Angelis[a,*]

[a] Computational Laboratory for Hybrid/Organic Photovoltaics (CLHYO), CNR-ISTM, via Elce di Sotto, I-06123, Perugia, Italy.

[b] Laboratory for Chemistry of Novel Materials, Universitè de Mons, Place du Park, 20, 7000 Mons, Belgium.

[c] Center for Nano Science and Technology @Polimi, Istituto Italiano di Tecnologia, via Giovanni Pascoli 70/3, 20133, Milan, Italy

[d] Dipartimento di Fisica, Politecnico di Milano, Piazza L. da Vinci, 32, 20133 Milano, Italy.

[e] University of Oxford, Clarendon Laboratory, Parks Road, Oxford, OX1 3PU, United Kingdom.

E-mail: Claudio.QUARTI@umons.ac.be; filippo@thch.unipg.it

EXPERIMENTAL METHODS

Sample Preparation. Devices for external quantum efficiency measurements based on $MAPbI_3$ were fabricated following previously published methods from our group. A thorough description of the fabrication and characterization of the device properties based on this procedure can be found in Ref. [1a]. In brief, fluorine-doped tin oxide (FTO) coated glass substrates were cleaned sequentially in aqueous Alconox detergent (Sigma-Aldrich, no. 242985), de-ionised water, acetone (Sigma-Aldrich, no. 32201), and isopropanol (IPA, Sigma-Aldrich, no. 33539) in an ultrasonic bath, followed by exposure to oxygen plasma. The electron-selective contact was comprised of a bilayer of spin-coated TiO_x nanoparticles and spin-coated C_{61}-butyric acid methyl ester (PCBM, NanoC). The perovskite was formed by evaporating PbI_2 onto the PCBM under high vacuum, and converting it via spin-coating methylammonium iodide on top followed by annealing at 100°C for 120 minutes inside a nitrogen filled glovebox. The hole-selective contact was formed by spin-coating a layer of (2,2',7,7'-tetrakis(N,N-di-p-methoxyphenylamine)-9,9-spirobifluorene) (spiro-MeOTAD), from a solution containing 72.3 mg spiro-OMeTad, 28.8 uL 4-tert-butylpyridine, 17.5 uL of a stock solution of 520 mg mL-1 lithium bis(trifluoromethylsulphonyl)imide in acetonitrile, per 1 mL anhydrous chlorobenzene. Devices were completed by evaporating a gold top contact electrode under high vacuum through a shadow mask.

The device based on the mixed iodide/chloride perovskite light-harvester was fabricated on cleaned indium doped tin oxide (ITO) coated glass substrates A PEDOT:PSS (Heraeus,Clevios 4083) solution was filtered through a 0.2 μm PVDF filter and spin-coated onto the substrates (2500 rpm, 60s), which were then heated to 150°C for 10 minutes. The substrates were transferred a nitrogen-filled glovebox for the processing of subsequent layers. The perovskite film was prepared by first forming a solution of methylammonium iodide (synthesized according to a literature recipe)[1b] and lead chloride (Sigma-Aldrich, no. 268690) in a 3:1 molar ratio at 40 wt% in anhydrous dimethylformamide (DMF, Sigma-Aldrich, no. 227056). This solution was spin-coated onto the substrates (2000 rpm, 60s), left to stand at room temperature for 30 minutes, and then heated to 90°C for 90 minutes followed by 30 minutes at 100°C. PCBM was spin coated (1000 rpm, 60 s) on top of the perovskite layers from a 20 mg/ml solution in chlorobenzene, followed by spin-coating (1000 rpm, 60s) of an aluminium doped zinc oxide film from an IPA solution (Nanograde N-10X, 6039). Finally, aluminum contacts were thermally evaporated under vacuum through a shadow mask to define the contact

electrodes. The sample preparation for UV-Vis absorption measurements followed the method described above as for the perovskite formed from mixed-halide precursors using plain glass microscope slides for the substrates without any other layers.

UV-Vis Absorption. The variable temperature absorption spectra were collected using a spectrophotometer (Perkin Elmer Lambda 1050) and a continuous flow static exchange gas cryostat (Oxford Instruments) furnished with three chambers one inside the other. The sample is housed inside the internal chamber filled with either gaseous He or N_2 while the corresponding cryogenic liquid (He/N_2) is fluxed inside the second (middle) chamber which is thermally isolated from the external ambient by the third (external) chamber which is evacuated (~ 10^{-5} - 10^{-6} mbar). The temperature control of the sample is achieved regulating both the flux of liquid helium flowing and the current flowing into a resistor placed close to the sample holder acting as a heater.

External Quantum Efficiency Measurements. External quantum efficiency (EQE) measurements were performed by illuminating the samples with a chopped (105 Hz) quart-tungsten-halogen lamp through a monochromator and measuring the device current as a function of wavelength using a lock-in amplifier (Newport). During the measurements the samples were maintained in a evacuated (~10^{-5} mbar) cryostat that was resistively heated for temperature control. The power dispersion of the optical system illuminating the cryostat was calibrated against a Si reference diode to derive the relative EQE.

Current density-Voltage Measurements. The current density-voltage characteristics of solar cells were measured under simulated AM 1.5G 100 mW/cm^2 irradiance (class AAA Newport solar simulator) using a Keithley 2400. The light intensity was calibrated using a silicon reference cell with a certification traceable to NREL. Devices were stabilized for 10s at open-circuit before sweeping the voltage at a scan rate of 40 mV/s.

COMPUTATIONAL METHODS

Structural models for SOC-GW calculations. The following models have been used to estimate the SOC-GW band gap of the orthorhombic, tetragonal and cubic phases of $MAPbI_3$. For the orthorhombic phase, we employed the P_{nma} structure proposed by Baikie et. al., composed by four $MAPbI_3$ units and with cell parameters a=8.8362 Å, b=12.5804 Å, c=8.5551.[3] For the tetragonal phase, we employed a model consistent with the structure proposed by Kawamura et. al. (I_{4mcm})[4] and Stoumpos et. al. ($I4_{cm}$).[5] A similar structure, with

I_{4mcm} space group has been recently proposed by Weller et. al.,[6] that is in good agreement with our models. The model consist in four $MAPbI_3$ units and cell parameters $a=b$=8.8556 Å and c=12.66 Å.[7] The cubic structure is composed by a 2x2x2 supercell of $MAPbI_3$ chemical residues, with the cell paramer fixed to twice the experimental value ($a=b=c$=6.33 Å, as reported by Weber and Poglitsch).[7]

All the structures have been optimized at the DFT level of theory, with cell parameters fixed to the above-mentioned experimental values, in the planewave/pseudopotential framework. In the case of the cubic structure, we performed two optimizations: i) with inorganic atoms fixed in the cubic positions and organic atoms relaxed (SOC-GW band gap of 1.16 eV) and ii) with all atomic positions relaxed (SOC-GW band gap of 1.28 eV).

Structural relaxations have been carried out with PBE exchange correlation functional,[8] together with ultrasoft,[9] scalar relativistic pseudopotentials for the ion. Electron−ion interactions were described by ultrasoft pseudopotentials with electrons from Pb 5d, 6s, 6p; N and C 2s, 2p; H 1s; I 5s, 5p shells explicitly included in the calculations. We used 25 Ry and 200 Ry kinetic energy cutoff, respectively for the wavefunction and the density. The following k-point mesh for the sampling of the First Brillouin zone[10] have been used: 4x4x4 for the orthorhombic and tetragonal structures and 2x2x2 for the cubic structure.

SOC-GW. By following the procedure reported in our previous work,[11] SR-GW calculations were performed using norm-conserving pseudopotentials with an energy cutoff of 70 Ry defining the plane-waves used for representing the wave-functions. GW calculations including SOC[11] were performed by using ultrasoft[12] pseudopotentials and energy cut-offs of 45 and 280 for the wave-functions and charge densities, respectively. SR-GW calculations were performed developing polarizability operators on a basis sets obtained as explained in Ref. [13] using an energy cutoff of 3 Ry and selecting the 2000 (3500) most important basis vectors for the tetragonal and orthorhombic (cubic) phase. The self-energy expectation values are first obtained on imaginary frequency and then analytically continued on the real frequency axis fitting with a two poles expansion.[14] SOC-GW calculations were performed including 400 (800) Kohn-Sham states, of which the first 200 (400) are doubly occupied for the tetragonal and orthorhombic (cubic) phase. All the presented GW calculations have been performed sampling the Brillouin's zone at the Γ point only, although the starting DFT calculations and the long range parts of the dielectric matrices are evaluated using a regular 4x4x4 (2x2x2) mesh of k-points for the tetragonal and orthorhombic (cubic) phase.

Car-Parrinello Molecular Dynamics simulations. CPMD simulations[15] have been carried out with the same Hamiltonian parameters used for structural optimizations: PBE-exchange correlation potential, ultrasoft, scalar relativistic pseudopotential, 25/200 Ry cutoff energy respectively for the expansion of the wavefunction and of the density.

For simulating both the tetragonal and the cubic phase of $MAPbI_3$, we resort to two models constituted by 2x2x2 supercell of the tetragonal phase (384 atoms and 32 MA cations), with cell parameters fixed to the experimental values (a=b=8.8556 Å and c=12.66 Å).[7] It is worth to note that the use of shorter cell parameters than the equilibrium one in the case of the cubic phase does not affect significantly the results of the simulation, as explained within the main text. The simulation of the tetragonal phase has been performed at an average temperature of 320 K, for a total time simulation of 12 picoseconds, after few picoseconds of equilibration. We used real ionic masses, except for the hydrogens that were deuterated, fictitious masses of 500 a.u. for the electrons and a time step of 5 a.u. The simulation of the cubic phase has been performed at an average temperature of 650 K. In this case, we set all the atomic masses equal to 6 a.u., to speed up the simulation. This choice affect the kinetic of the simulation, resulting for instance in an artificial increasing the vibrational frequencies of the system, but it does not affect the force calculation, thus allowing to the system to explore the same conformation in the phase space in a shorter time. As a result of this artificial decrease of the atomic masses, the simulation has been performed using a fictitious electronic mass of 1000 a.u. and a total simulation of only 6 ps, after few ps of equilibration.

Evolution of the band gap during the CPMD simulations. The evolution of the band gap during the CPMD simulation has been performed as follows. One geometry for each 0.06 ps has been extracted from the trajectory of molecular dynamics, for both the simulation on the tetragonal and cubic structure. The band gap has been evaluated at DFT level, in the planewave/pseudopotential framework, using PBE exchange-correlation functional, 25/200 Ry kinetic energy cutoff respectively for the wavefunction and the density. In light of the large dimension of the crystalline cell from the CPMD simulation (384 atoms), the k-point mesh of the first Brillouin zone was restricted only to the Gamma point. Calculation of the band has been calculated both at the scalar-relativistic and considering spin-orbit coupling, respectively using

scalar-relativistic and full-relativistic pseudopotentials. All calculations have been performed with the quantum-espresso suite of programs.[16]

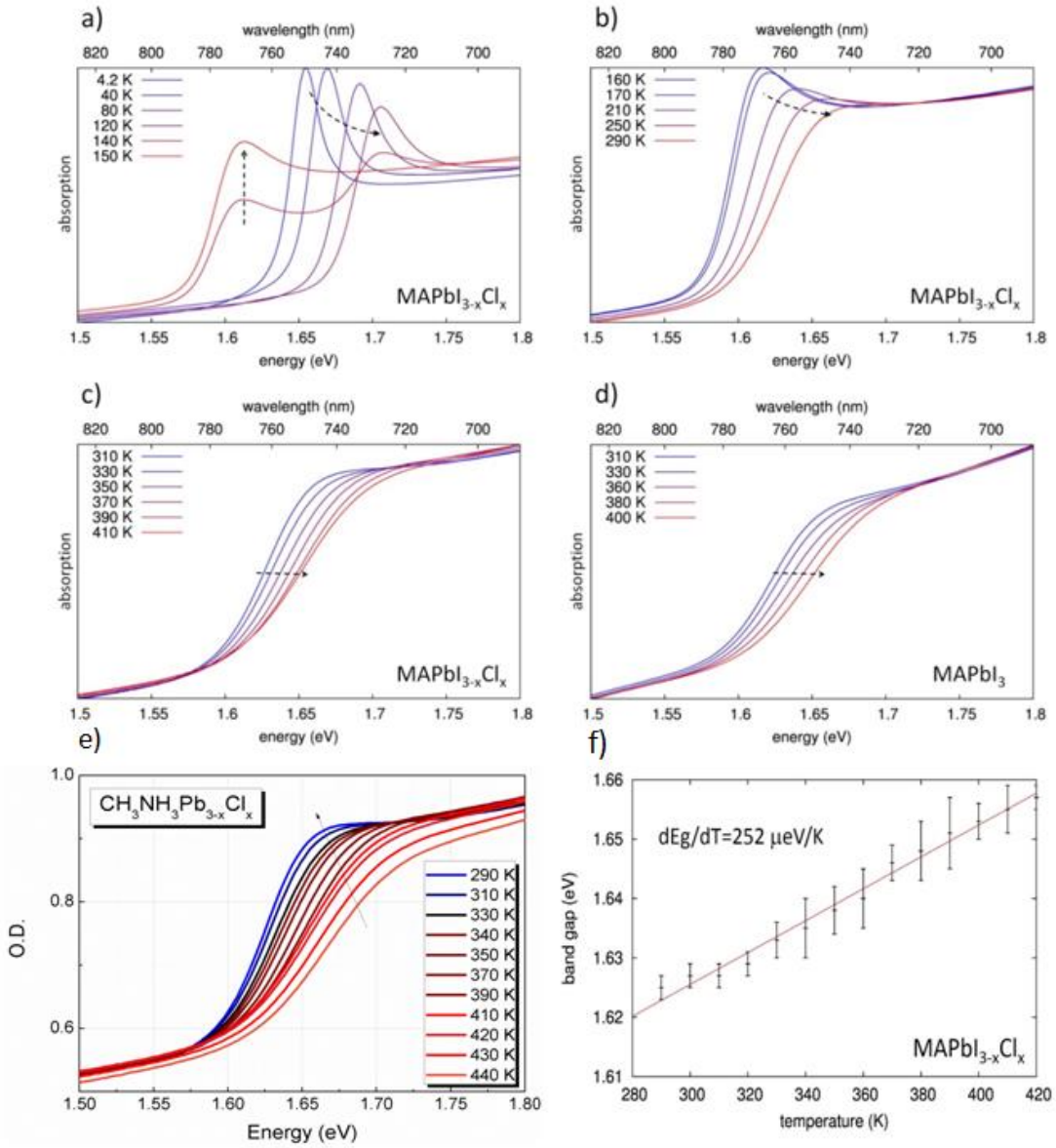

Figure SI1. Comparison of the optical properties of MAPbI3 and of $MAPbI_{3-x}Cl_x$ films.

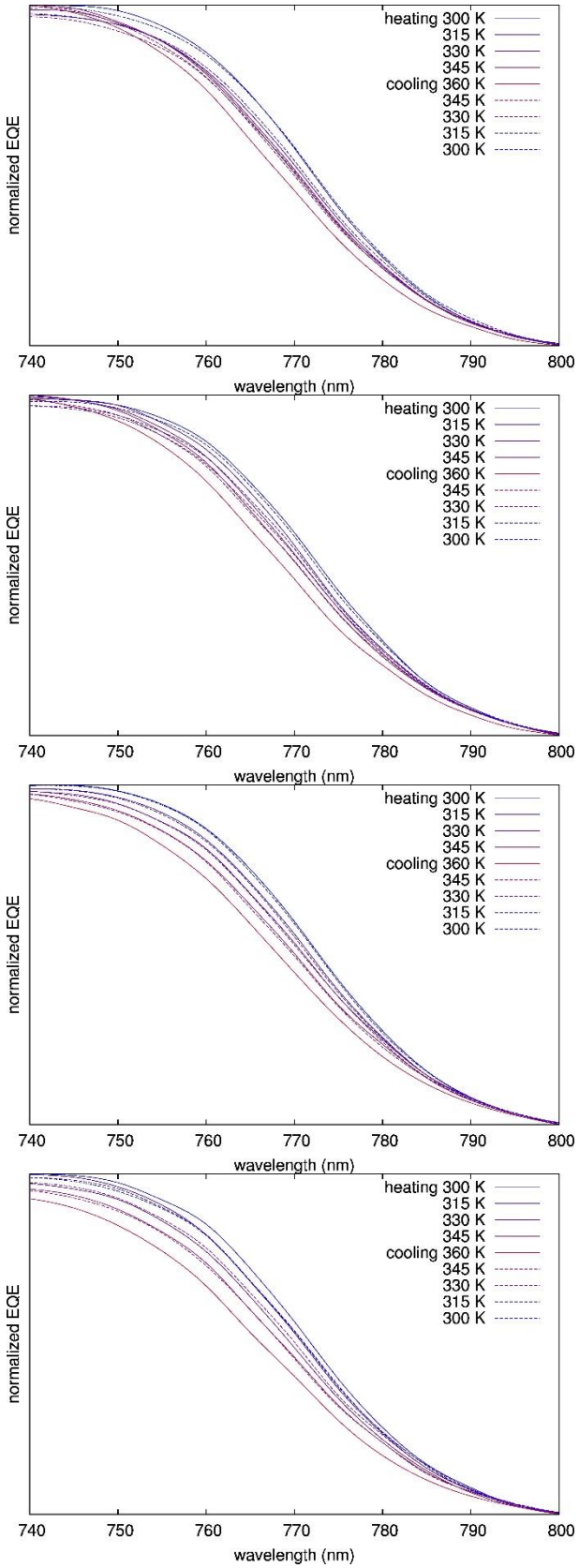

Figure SI2. Normalized EQE of several devices in heating and cooling back across several $MAPbI_3$ based devices.

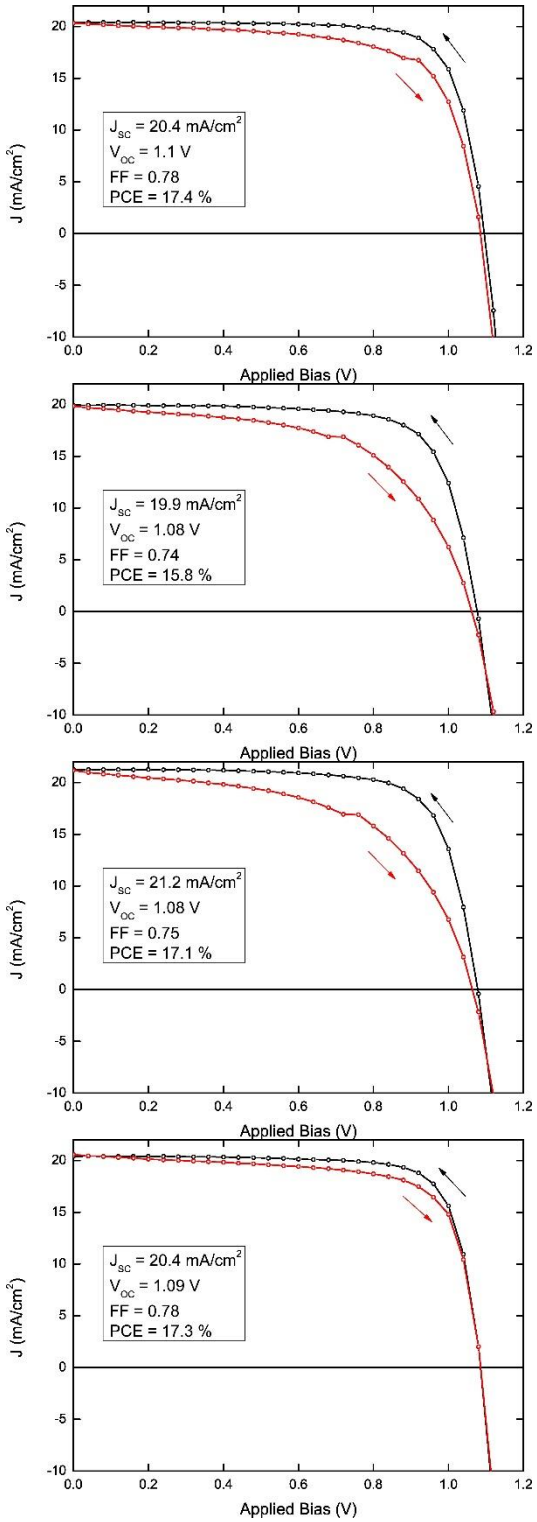

Figure SI3. JV measurements of the $MAPbI_3$-based devices with the EQE reported in Figure SI2.

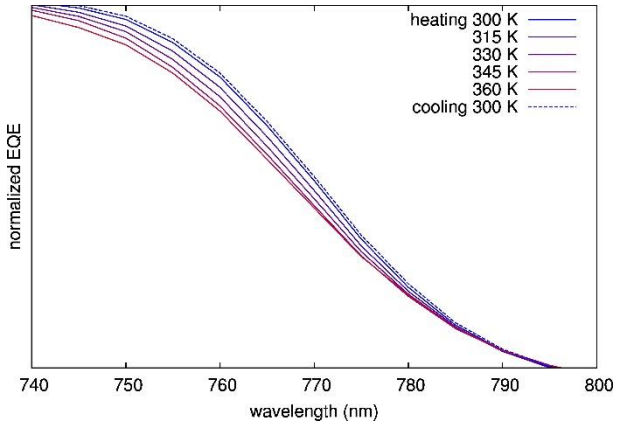

Figure SI4. Normalized External Quantum Efficiency of several devices in heating and cooling back across one $MAPbI_{3-x}Cl_x$ based device.

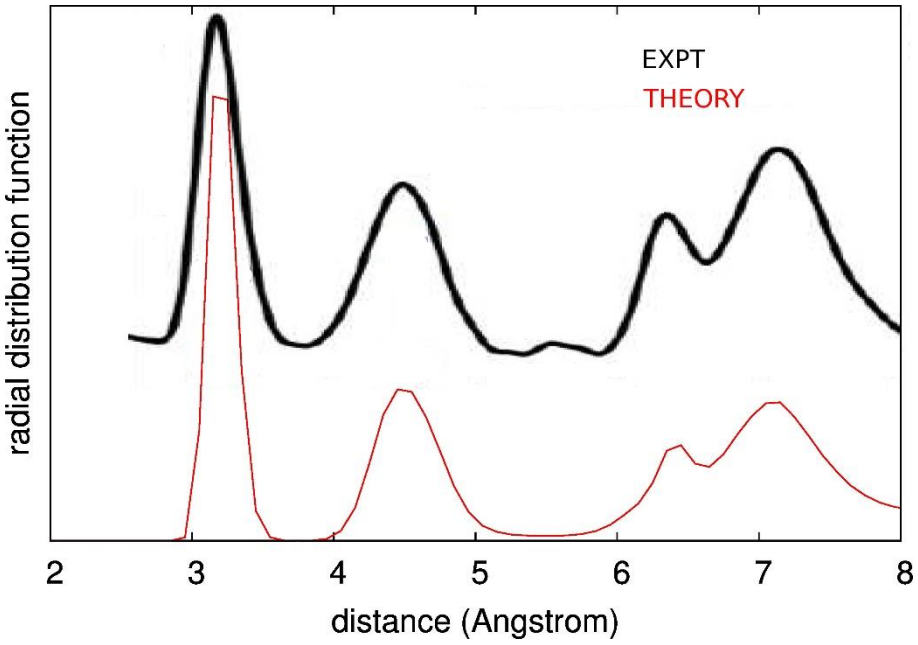

Figure SI5. Theoretical radial distribution function computed for $MAPbI_3$ from molecular dynamics, compared with the experimental data from Ref. [17].

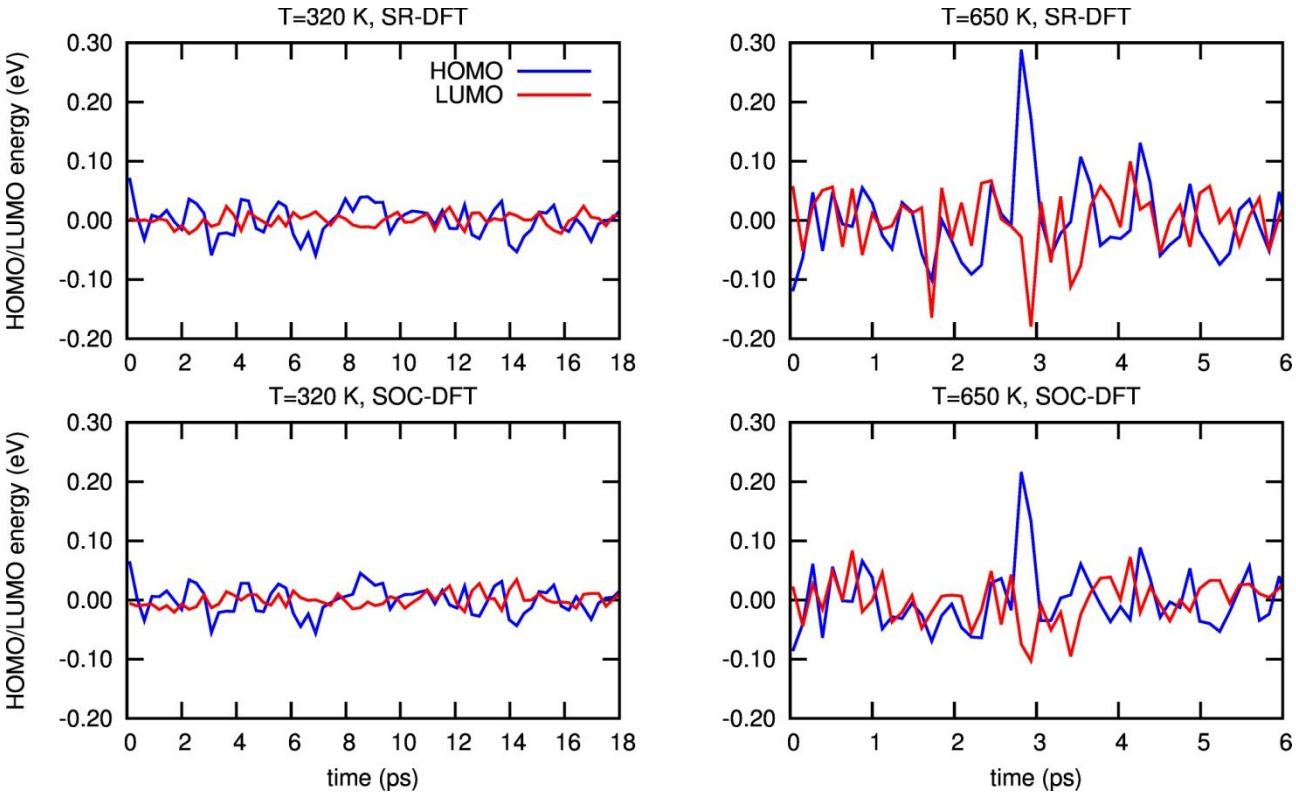

Figure SI5. Time evolution of the HOMO and LUMO of MAPbI3 during the dynamics simulations calculated by SR- and SOC-DFT.

Bibliography

1. a) Tao, C., S. Neutzner, L. Colella, S. Marras, A.R.S. Kandada, M. Gandini, M. De Bastiani, G. Pace, L. Manna, M. Caironi, C. Bertarelli, and A. Petrozza, 17.6% stabilized efficiency in low-temperature processed planar perovskite solar cells. *Energy and Environmental Science*, 2015. **8**, 2365-2370; b) Lee, M.M., J. Teuscher, T. Miyasaka, T.N. Murakami, and H.J. Snaith, Efficient Hybrid Solar Cells Based on Meso-Superstructured Organometal Halide Perovskites. *Science*, 2012. **338**, 463-467.
2. Xiao, Z., C. Bi, Y. Shao, Q. Dong, Q. Wang, Y. Yuan, C. Wang, Y. Gao, and J. Huang, Efficient, high yield perovskite photovoltaic devices grown by interdiffusion of solution-processed precursor stacking layers. *Energy and Environmental Science*, 2014. **7**, 2619-2623.
3. Baikie, T., Y. Fang, J.M. Kadro, M. Schreyer, F. Wei, S.G. Mhaisalkar, M. Graetzel, and T.J. Whitec, Synthesis and Crystal Chemistry of the Hybrid Perovskite $(CH_3NH_3)PbI_3$ for Solid-State Sensitised Solar Sell Applications. *J. Mater. Chem. A*, 2013. **1**, 5628–5641.
4. Kawamura, Y., H. Mashiyama, and K. Hasebe, Structural study on cubic-tetragonal transition of $CH_3NH_3PbI_3$. *Journal of Physical Society of Japan*, 2002. **71**, 1694-1697.
5. Stoumpos, C.C., C.D. Malliakas, and M.G. Kanatzidis, Semiconducting Tin and Lead Iodide Perovskites with Organic Cations: Phase Transitions, High Mobilities, and Near-Infrared Photoluminescent Properties. *Inorg. Chem.*, 2013. **52**, 9019−9038.

6. Weller, M.T., O.J. Weber, P.F. Henry, A. Di Pumpo, and T.C. Hansen, Complete structure and cation orientation in the perovskite photovoltaic methylammonium lead iodide between 100 and 352 K. *Chemical Communications*, 2015. **51**, 4180-4183.
7. Poglitsch, A. and D. Weber, Dynamic Disorder in Methylammoniumtrihalogenoplumbates (II) Observed by Millimeterwave Spectroscopy. *J. Chem. Phys.*, 1987. **87**, 6373-6378.
8. Perdew, J.P., K. Burke, and M. Ernzerhof, Generalized Gradient Approximation Made Simple. *Physical Review B*, 1996. **77**, 3865-3868.
9. Vanderbilt, D., Soft Self-Consistent Pseudopotentials in a Generalized Eigenvalue Formalism. *Physical Review B*, 1990. **41**, 7892-7895.
10. Monkhorst, H.J. and J.D. Pack, Special Points for Brillouin-Zone Integrations. *Physical Review B*, 1976. **13**, 5188–5192.
11. Umari, P., E. Mosconi, and F. De Angelis, Relativistic GW calculations on $CH_3NH_3PbI_3$ and $CH_3NH_3SnI_3$ Perovskites for Solar Cell Applications. *Sci. Rep.*, 2014. **4**, 4467.
12. Vanderbilt, D., Soft self-consistent pseudopotentials in a generalized eigenvalue formalism. *Phys. Rev. B*, 1990. **41**, 7892-7895.
13. Umari, P., G. Stenuit, and S. Baroni, GW quasiparticle spectra from occupied states only. *Phys. Rev. B*, 2010. **81**, 115104.
14. Rieger, M.M., L. Steinbeck, I.D. White, H.N. Rojas, and R.W. Godby, The GW space-time method for the self-energy of large systems. *Comp. Phys. Comm.*, 1999. **117**, 211-228.
15. Car , R. and M. Parrinello, Unified Approach for Molecular Dynamics and Density-Functional Theory. *Physical Review Letters*, 1985. **55**, 2471–2474.
16. Giannozzi, P., S. Baroni, N. Bonini, M. Calandra, R. Car, C. Cavazzoni, D. Ceresoli, G.L. Chiarotti, M. Coccioni, I. Dabo, A. Dal Corso, S. de Gironcoli, S. Fabris, G. Fratesi, R. Gebauer, U. Gerstmann, C. Gougoussis, A. Kokalj, M. Lazzeri, L. Martin-Samos, N. Marzari, F. Mauri, R. Mazzarello, S. Paolini, A. Pasquarello, L. Paulatto, C. Sbraccia, S. Scandolo, G. Sclauzero, A.P. Seitsonen, A. Smogunov, P. Umari, and R.M. Wentzcovitch, QUANTUM ESPRESSO: a Modular and Open-Source Software Project for Quantum Simulations of Materials. *Journal of Physics: Condensed Matter*, 2009. **21**, 395502.
17. Choi, J.J., X. Yang, Z.M. Norman, S.J.L. Billinge, and J.S. Owen, Structure of Methylammonium Lead Iodide Within Mesoporous Titanium Dioxide: Active Material in High-Performance Perovskite Solar Cells. *Nano Letters*, 2013. **14**, 127-133.